Pharmacogn. Mag.
A multifaceted peer reviewed journal in the field of Pharmacognosy and Natural Products
www.phcog.com | www.phcog.net

ORIGINAL ARTICLE

Ethyl Acetate Fraction of *Anethum graveolens* Seeds Exerts an Antiproliferative Effect by Inhibiting Anti-apoptotic Proteins in MCF-7 and PC-3 Cells: An *in vitro* and Molecular Docking Study

Furkhan Ahmed Mohammed[1], Waseem Mohammed Abdul[2], Md Tabish Rehman[3], Mohamed F. AlAjmi[3], Fareeduddin Quadri Syed[1], Muqtadir Baig Mirza[1], Ayman I. Elkady[1,4], Anzarul Haque[5], Muhummadh Khan[1,6]

[1]Department of Biological Science, Faculty of Science, King Abdulaziz University (KAU), Jeddah, Saudi Arabia, [2]Department of Microbiology, Mumtaz Degree and PG College, Osmania University, Hyderabad, India, [3]Department of Pharmacognosy, College of Pharmacy, King Saud University, Riyadh, Saudi Arabia, [4]Department Zoology, Faculty of Science, Alexandria University, Alexandria, Egypt, [5]College of Pharmacy, Department of Pharmacognosy Prince Sattam bin Abdul Aziz university, Alkharj, [6]Genetics and Biotechnology Section, Department of Biology, King Abdulaziz University (KAU), Jeddah, Saudi Arabia

Submitted: 18-Dec-2020 Revised: 10-Feb-2021 Accepted: 18-Mar-2021 Published: 10-Jun-2021

ABSTRACT

Background: *Anethum graveolens* seeds have therapeutic benefits, which may be a potential approach to the treatment of different cancers. **Objectives:** We investigated, the antiproliferative effect of ethyl acetate fraction of dill (EAFD), on MCF-7 and PC-3 cell lines and its two most active components, anethole and carvone by molecular docking analysis. **Materials and Methods:** *In-vitro* assays, like cell viability assay and measurement of reactive oxygen species, were performed besides performing Giemsa stain and other fluorescent stains; JC-1 dye, dual mixed stain ethidium bromide/acridine orange and 4,6-diamidino-2-phenylindole stain to study morphological characteristics, including molecular docking analysis. EAFD concentrations (0.2, 0.4, 0.6, 0.8, 1.0 mg/ml) were used. **Results:** The EAFD prominently inhibited the proliferation of MCF-7 cells and PC-3 cells by dose-dependent and time-dependent methods. Increased exposure of EAFD to MCF-7 and PC-3 cells increases the level of intracellular oxidative stress. Similarly, EAFD exposure confirms the morphological alternations such as cell shrinkage, membrane disruption, nuclear condensation, and blebbing in phase-contrast microscopy and even fluorescent microscopy stains can lead to mitochondrial membrane degradation, chromatin condensation, nuclear fragmentation. Analyses of docking results suggest that anethole and carvone bind to the hydrophobic patches of Bcl-2 and Bcl-xL through hydrophobic interactions. **Conclusion:** The EAFD may be antiproliferative activity and leading to pro-apoptotic cell death. Molecular docking analysis of Bcl-2 and Bcl-xL anti-apoptotic protein indicated that the antiproliferative activity and pro-apoptotic cell deaths by EAFD are possibly due to inhibition of these proteins.

Key words: *Anethum graveolens,* anti-proliferation, apoptosis, cancer, herbal medicine, intracellular oxidative stress, molecular docking

SUMMARY

- The current study revealed that the antiproliferative effect of ethyl acetate fraction of dill (EAFD) on MCF-7 and PC-3 cell lines. Moreover, it is two most active components, anethole, and carvone through molecular docking analysis. *In-vitro* assays and other fluorescent stains were performed JC-1 dye, and 4,6-diamidino-2-phenylindole stain was used to study morphological features of pro-apoptotic cell death, besides molecular docking analysis. The EAFD prominently inhibited the proliferation of MCF-7 and PC-3 cells. Similarly, EAFD exposure confirms that morphological alternations can lead to mitochondrial membrane degradation, chromatin condensation by fluorescent microscopy stains. This result suggests that EAFD may be an antiproliferative activity that causes pro-apoptotic cell death. Bcl-2 and Bcl-XL anti-apoptotic protein molecular docking analysis showed that antiproliferative activity and pro-apoptotic cell deaths by EAFD could be due to inhibition of these proteins.

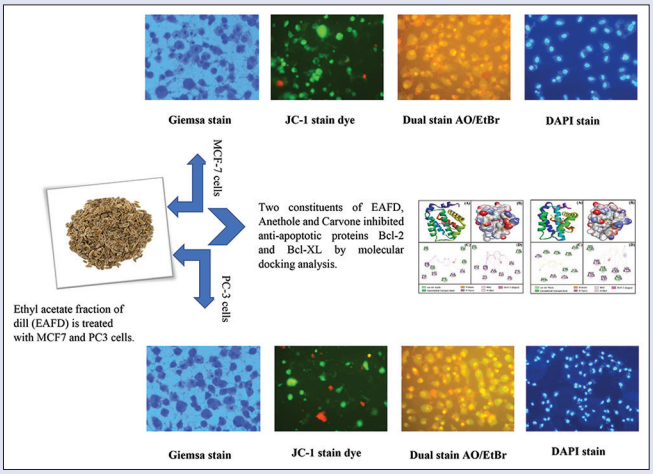

Abbreviations Used: EAFD: Ethyl Acetate Fraction of Dill; MTT: 3-(4,5-Dimethylthiazol-2-yl)-2,5-diphenyltetrazolium bromide; PBS: Phosphate buffer saline; DMSO: Dimethyl sulfoxide; EDTA: Ethylene-diamine-tetra-acetic acid; MMFF: (Merck Molecular Force Field); LGA: (Lamarckian Genetic Algorithm).

Correspondence:

Dr. Furkhan Ahmed Mohammed,
Department of Biological Science, Faculty of Science, King Abdulaziz University (KAU), PO. Box 80203, Jeddah, Saudi Arabia.
E-mail: furkhanmohammed11@gmail.com
DOI: 10.4103/pm.pm_538_20

Access this article online
Website: www.phcog.com
Quick Response Code:

INTRODUCTION

Cancer is a cluster of diseases, arising due to the transformation of normal healthy cells into tumor cells with altered cellular mechanisms; it is a multistage process in which, the cell loses the capacity to control its proliferation rate and actively divides in an uncontrolled manner.[1] It usually goes from a pre-cancer lesion to a malignant

Cite this article as: Mohammed FA, Abdul WM, Rehman MT, AlAjmi MF, Syed FQ, Mirza MB, *et al*. Ethyl acetate fraction of *Anethum graveolens* seeds exerts an antiproliferative effect by inhibiting anti-apoptotic proteins in MCF-7 and PC-3 cells: An *in vitro* and molecular docking study. Phcog Mag 2021;17:S105-13.

tumor, until the underlying mechanism is fully opened, by controlling the progression/growth/metastasis and endurance of malignant cells.[2] There were about 18.1 million cancer cases in the year 2018 alone globally, of which 9.6 million lead to death. From the year 2005–2015, cancer cases had been raised by 33%, with population aging subsidizing 16%, alterations in age-specific rates by 4%, and finally population growth by 13%. According to an estimate, there would be around 13–17 million deaths in 2030.[3] In particular, breast and prostate cancer-associated mortalities are increasing at an alarming rate. In men, the most widely documented cancer universally is prostate cancer; while among females, the majority of acknowledged cases were breast cancer.[4] Currently, the treatment of cancer has relied on chemotherapy and radiotherapy for metastasized tumors; moreover, surgical intervention is found to be the only solution in case of localized tumors although, these have various life-threatening side effects.[5]

Conventionally, plants with identified therapeutic potency are used in the treatment of a variety of diseases since time immemorial. The practice of using curative herbal plants has a significant prominence, specifically for their advantages as medicinal herbs with negligible or no side effects.[6] *Anethum graveolens* L. (dill), (Apiaceae) is a kind of one of popular culinary and ancient aromatic herbs. Dill seeds comprise of following components-essential oils; 15.68% of fatty oil proteins, 14.80% of fiber, 9.8% of ash, 8.39% of moisture, 36% of carbohydrates along with mineral elements such as magnesium, phosphorus, sodium, calcium, potassium, niacin, and Vitamin A in trace amounts.[7] The *A. graveolens* possess a wide range of medicinal properties which include: Antihyperlipidemic,[8] antidiabetic,[9] anti-inflammatory, and analgesia.[10] It also contains a prominent source of antioxidants.[11] The typical medicinal properties of dill reported from the traditional perspective include gastrointestinal ailments such as flatulence, indigestion, stomachache and colic carminative, stomachic, and diuretic.[12]

In normal conditions, apoptosis is tightly regulated by an excellent play between pro-apoptotic and anti-apoptotic proteins, belonging to the Bcl-2 family.[13] These proteins are localized at the outer membrane of mitochondria and are sensitive to any changes in the homeostatic state of a healthy condition. On receiving an appropriate signal, apoptosis is initiated through the release of cytochrome 'C' from the mitochondrial inner membrane.[14] In many cancers, overexpression of anti-apoptotic Bcl-2 proteins leads to the inhibition of cytochrome 'C' release and hence inhibition of apoptosis. The three-dimensional structure of Bcl-2 and Bcl-xL anti-apoptotic proteins comprises eight α-helices organized into four domains, namely BH1, BH2, BH3, and BH4. The initiation of apoptosis takes place when the BH3 domain of anti-apoptotic proteins interacts with pro-apoptotic proteins (e.g. Bad, Bod, Bik, and so forth.) which contain only the BH3 domain.[15,16] Thus, the identification of effective inhibitors against anti-apoptotic proteins such as Bcl-2, Bcl-xL, and Mcl-1 is a promising approach to fight cancer.

In another study, the antiproliferative, pro-apoptotic and cell cycle arrest effects of ethyl acetate fraction of dill (EAFD) on investigated on HepG2 cells are reported.[17] Various studies investigated the biological activities of *A. graveolens* seeds to date, but no study addresses the antiproliferative activity of the dill seeds on MCF-7 and PC-3 cells. In addition, the two most active components of EAFD, i.e., anethole and carvone, are demonstrated by molecular docking analysis.

MATERIALS AND METHODS

Preparation and Extraction of medicinal herb *Anethum graveolens* seeds

Anethum graveolens seeds were bought from the local market of Jeddah, Kingdom of Saudi Arabia. The identification and authentication of seeds were performed by the experts of Taxonomy (Specimen voucher number: *A. graveolens* L. dill #AG17600) at the Herbarium of Department of Biology, Faculty of Sciences, King Abdulaziz University, Jeddah, Kingdom of Saudi Arabia. In our previous study, we have clearly described the detailed protocol method of extraction and fractionation of EAFD.

Cell culture

The MCF-7 and PC-3 cells were acquired from King Fahad Center for Medical Research, King Abdulaziz University, Kingdom of Saudi Arabia. These cell lines were originally obtained from American Type Culture Collection ATCC (USA). The cells were grown in Dulbecco's Modified Eagle Medium (DMEM) (HyClone™, catalog # SH30022.01) supplemented with 10% fetal bovine serum, (HyClone™, catalog # SH30910.03HI) and 1% Penicillin-streptomycin antibiotics (HyClone™, catalog # SV30010) under a dampened environment comprising 5% CO_2 and 95% air at 37°C.

Cell Viability 3-(4,5-Dimethylthiazol-2-yl)-2, 5-diphenyltetrazolium bromide assay

The effect of EAFD on MCF-7 and PC-3 cells was evaluated by the 3-(4,5-Dimethylthiazol-2-yl)-2,5-diphenyltetrazolium bromide (MTT) assay kit (Cayman Chemicals, USA) following the manufacturer instructions. Concisely, 96 well plates were seeded at a density of 7×10^3 cells/well (PC-3) and 8×10^3 cells/well (MCF-7) in 100 µl of culture medium (DMEM) and incubated overnight. The MCF-7 and PC-3 cells were treated with increasing concentrations (0.2, 0.4, 0.6, 0.8, 1.0 mg/ml) of EAFD for 48 h. Finally, 10 µl of MTT (freshly prepared) was supplemented to each well and mixed slightly for a minute on an orbital shaker. Following this, the cells were incubated for about 3–4 h at 37°C in a CO_2 incubator. Furthermore, the formazan granules formed in the cells appeared as dark crystals at the base of the wells. Finally, 100 µl of crystals dissolving solution was put in every well and incubated for 10 min at 37°C in a carbon dioxide incubator. The optical density of each sample was evaluated at 570 nm with the help of a microplate reader (BioTek Synergy H.T.X.). The IC_{50} (50% inhibitory concentration) and the effect of EAFD on growth inhibition were assessed as percentage cell viability, where control (dimethyl sulfoxide-treated) cells were taken as 100% viable.[18]

Measurement of reactive oxygen species

The reactive oxygen species (ROS) produced was monitored with the help of the fluorescence probe, DCFH-DA (Cayman Chemicals), following the manufacturer's instructions. Briefly, 8×10^3 cells/well (MCF-7) and 7×10^3 cells/well (PC-3) cells in 96 well plates were seeded and further treated with increasing concentrations of EAFD for about 24-h, as explained above. Following this, 2 µl of DCFH-DA is added to each well and incubated for 30 min. The measurement of fluorescence is done with the help of a microplate ELISA reader at 485 nm excitation and 528 nm emission (Synergy/HTX. multimode Reader, BIOTEK).

Giemsa staining for morphological changes

The 24 well plates were used for Giemsa staining in which, the MCF-7 cells are seeded 5×10^4 and PC-3 cells are seeded 2×10^5 and kept overnight for cell attachment. After the attachment, with concentrations of EAFD, the cells were treated for 24 h. Cells are stained by Giemsa stain, by washing the wells with phosphate buffer saline (PBS), which are then fixed with 3.7% of paraformaldehyde (Sigma-Aldrich) for about 10 min at room temperature. Then the attached cells were washed with PBS and are stained with 250 µl of Giemsa. At the magnifications of ×100, ×200, and ×400 of a phase-contrast microscope (Leica, Wetzlar, Germany), the cells were observed after the incubation.

Mitochondrial membrane potential (ΔΨm) (JC-1) staining dye

Mitochondrial membrane potential (MMP) was performed through JC-1 dye (5, 5', 6, 6'-Tetrachloro-1, 1', 3, 3'-tetraethylbenzimi dazolylcarbocyanineiodide), it is a cytofluorimetric dye with lyophilic and cationic ions (Cayman Chemicals, USA). The JC-1 demonstrates the potential dependent collection in the mitochondria, pointed through a fluorescence emission stimulated from red to green. Briefly, MCF-7 cells and PC-3 cells were seeded 5×10^4 cells and 2×10^5, respectively, within 24 well plates and allowed to grow throughout the night and with the treatment of different concentrations of EAFD for about 24 h. The EAFD treated cells were double washed with PBS and further incubated with the JC-1 cocktail solution (including virgin DMEM media, JC-1 buffer solution, and JC-1 stain), for about 10–20 min at 37°C. Lastly, the fluorescence microscope was used to capture the fluorescent signals (Leica, Wetzlar, Germany).

Acridine orange and ethidium bromide dual staining method

Morphological detection of apoptotic, viable, and necrotic cells is made using DNA binding dyes; "AO" and "EtBr" acquired from Sigma, USA. When added into DNA, both viable and nonviable absorbed by Acridine orange (AO) dye, which releases green fluorescence. The nonviable cells taken up by ethidium bromide (EtBr) dye while viable cells are excluded from it, by emitting red fluorescence after adding into DNA. Subsequently, both the PC-3 cells and MCF-7 cells in a chamber slide were seeded with a density of 5×10^4 cells, in each chamber area, the cells were grown up to 60%–70% confluence. Following this, the cells were treated under different concentrations of EAFD for about 24 h. Furthermore, the MCF-7 cells and PC-3 cells were stained with a mixture of AO (5 μg/ml) and EtBr (5 μg/ml) at room temperature for 20 min. The cells were directly observed under the fluorescent microscope at ×400 (Leica, Wetzlar, Germany).

4,6-diamidino-2-phenylindole Staining for nuclear apoptotic assay

The nucleus of an apoptotic cell undergoes some morphological changes and it is analyzed using 4,6-diamidino-2-phenylindole (DAPI; Sigma Aldrich). A fluorescent nuclear dye that binds to DNA brings out changes in the nucleus, nuclear fragmentation, and condensation of chromatin. The MCF-7 and PC-3 cells are seeded with 5×10^4 cells and 2×10^5 cells in 24 well plates, respectively and left overnight for the attachment. Succeeding attachment, the cells were treated with different concentrations of EAFD for 24 h. After that, the cells were washed at room temperature, fixed and then stained with a DAPI (Sigma Aldrich) solution for about 10 min. The cells that were stained are then washed with PBS and examined under the fluorescence microscope at ×400 (Leica, Wetzlar, Germany).

Molecular docking

The potential of the two most abundant constituents of *Anethum graveolens* L. (Dill), namely anethole and carvone, was evaluated by performing molecular docking. The proteins Bcl-2 and Bcl-xL modulate the fate of cells by acting as an inhibitor of apoptosis and hence promoting proliferation were chosen as potential targets of anethole and carvone. The 2D structures of anethole and carvone were drawn in ChemSketch and their geometries were cleaned using Charmm forcefield.

The 3D coordinates of Bcl-2 (PDB ID: 2W3L) and Bcl-xL (PDB ID: 2YXJ) were retrieved from PDB-RCSB databank. The X-ray crystal structure of Bcl-2 bound with DRO (1-(2-[(3S)-3-(aminomethyl)-3,4-dihydroisoquinolin-2 (1H)-yl] carbonylphenyl)-4-chloro-5-methyl-N,N-diphenyl-1H-pyrazole -3-carboxamide) was solved to 2.10 Å resolution.[19] Likewise, the X-ray crystal structure of Bcl-xL bound with N3C (4-4-[(4'-chlorobiphenyl-2-yl) methyl] piperazin-1-yl-N-[4-(1R)-3-(dimethylamino)-1-[(phenylthio) methyl] propylamino)-3 nitrophenyl] sulfonyl} benzamide) was reported at 2.20 Å.[20] It was before molecular docking; the proteins were preprocessed by the removal of crystallographic water molecules and any other hetero atoms, the addition of hydrogen atoms, assigning proper bond order and defining rotatable bonds as briefed.[21] A network of H-bonds was created and the energy of protein was minimized using Merck Molecular Force Field forcefield. A grid-box of 27 × 30 × 25 Å centered as 39 × 28×-12 Å and 28 × 33 × 26 Å centered as −8× −17 × 9 Å with 0.375 Å spacing was defined as a conformation search space for the binding of ligands to Bcl-2 and Bcl-xL, respectively. Finally, molecular docking between ligands and proteins was performed using Autodock4.2 as described earlier.[22] Molecular docking was performed using lamarckian genetic algorithm and Solis and Wets local search methods. The initial torsions, position, and orientations of ligands were set randomly. For each docking run, a maximum of 2.5×10^6 calculations were enumerated after setting the population size at 150 and a translational step of 0.2 Å. Quaternion and torsion steps were set to 5. Discovery Studio (Accelrys) was employed to analyze the docking results and prepare figures. Binding affinities of anethole and carvone for Bcl-2 and Bcl-xL was determined from their respective binding energies (ΔG) using the below:[23]

$$\Delta G = -RTlnK_d$$

Where R was Boltzmann gas constant (=1.987 kcal/mol/K) and T was the temperature (=298 K).

Statistical analysis

For comparing the variances between the control and treated groups cells, statistical analysis was accomplished through ordinary one-way ANOVA (non-parametric) and unpaired Student's test (two-tailed). The outcome was represented as the mean ± standard error of the mean of triplicates performed by an average of three independent experiments ($n = 3$). P value is exhibited as $^*P < 0.05$, $^{**}P < 0.001$, $^{***}P < 0.0001$ and was considered as statistically significant.

RESULTS

Ethyl acetate fraction of dill anti-proliferation and inhibition of growth of MCF-7 and PC-3 cell lines

MTT assay was performed by using MCF-7 and PC-3 cell lines for determining the anti-proliferation activity of EAFD with different concentrations (0.2, 0.4, 0.6, 0.8, 1.0 mg/ml) in both control dose and in a time-dependent manner. However, the treatment of the MCF-7 cells for 24 h incubation period shows a minute increase in inhibition of cells treated with EAFD at low concentrations followed by a gradual increase at higher concentrations, the viable cells of MCF-7 cells were reduced from 91% (0.2 mg/ml) to 30% (1.0 mg/ml) in 24 h of treatment. At higher concentrations of 1.0 mg/ml, there was a significant decrease in the proliferation of cells. Whereas, when MCF-7 cells were treated for 48 h, the inhibition of cells was more significant with lesser P value, i.e., ($P < 0.0001$) value compared to 24 h of incubation. The percentage of viable cell decrease in 48 h is from 30% (0.2 mg/ml) to 15% (1.0 mg/ml), as depicted in Figure 1a and b. Another cell line PC-3, when treated with EAFD for 24 h, has shown an increase in the percentage of cell inhibition post-treatment at higher doses. The viable cells of PC-3 decreased significantly from 87% (0.2 mg/ml) to 25% (1.0 mg/ml). Furthermore, in 48 h treatment, the inhibition of PC-3 cells shows a more significant

P value, i.e., ($P < 0.0001$) value as compared to 24 h treatment. The percentage of viable cells present in 48 h of incubation are tremendously decreased from 33% (0.2 mg/ml) to 10% (1.0 mg/ml), as depicted in Figure 2a and b. IC_{50} of MCF-7 cells at 24 h was (0.7323 mg/ml), 48 h (0.5569 mg/ml). Moreover, IC_{50} of PC-3 cells was 24 h (0.59 mg/ml), 48 h (0.3741 mg/ml) was calculated.

Ethyl acetate fraction of dill induces reactive oxygen species production

The role of an intracellular generation of ROS level (DCFH-DA stain) in inducing the pro-apoptotic cell death in cancer cells after EAFD treatment was assessed. The two cell lines MCF-7 and PC-3 were used for evaluating the effect of EAFD at various concentrations (0.2, 0.4, 0.6, 0.8, 1.0 mg/ml) associated with a control in a 24 h of incubation period with both dose and time-dependent method. At first, the PC-3 cells were treated with EAFD and it displayed a gradual increase in ROS production with an increase in the dose (0.6, 0.8, 1.0 mg/ml). In PC-3 cells, after treatment, quite significant '*P*' value was obtained ($P < 0.001$), as shown in Figure 3a. On the other hand, MCF-7 cells treated with EAFD indicates that there is an increase in the ROS levels with increased dosages (0.4, 0.6, 0.8, 1.0 mg/ml), resulting in more significant *P* value, i.e., ($P < 0.0001$), as depicted in Figure 3b. The exposure of MCF-7 and PC-3 with EAFD, resulting in oxidative stress and apoptotic cell death may be responsible for EAFD to act as an anticancer agent.

Morphological changes in ethyl acetate fraction of dill treated cells by Giemsa staining

The EAFD treatment revealed the distinguishing apoptotic changes in MCF-7 and PC-3 cells when they are treated with different concentrations of 0.2, 0.4, 0.6, 0.8, 1.0 mg/ml. Both MCF-7 and PC-3 cells are stained with Giemsa staining at 24 h of incubation, the morphological changes were observed like cells shrinkage, membrane disruption, nuclear condensation, and blebbing in phase contrast microscope with ×100, ×200, and ×400 magnification as shown in Figure 4a and b. The most noticeable detachment and cell death of MCF-7 cells and PC-3 cells monolayer were observed in 0.8 and 1.0 mg/ml of EAFD in ×400.

Ethyl acetate fraction of dill induces mitochondrial membrane potential (JC-1) by fluorescent staining dye

We demonstrated MMP, the MCF-7 and PC-3 cells treated with EAFD in different concentrations. With the loss of MMP, there was an increase in EAFD concentration with decreases in red fluorescence. As seen in control, MMP (JC-1 dye) concentration has reached to the mitochondrial matrix; it shows J-aggregates (red fluorescence). Nevertheless, in the EAFD treated cells MCF-7 and PC-3 were interrupted in the mitochondrial membrane, the JC-1 dye in the mitochondria leads to stop accumulation. Thus, indicating that malfunction of MMP; finally, JC-1 dye was distributed all over the cell which preceding to a from red (J-aggregates) to green fluorescence (JC-monomers) shift, then EAFD concentrations dependent increased in treatment of MCF-7 and PC-3 cells were observed under fluorescent microscopy ×400 Figure 5a and b.

Detection of apoptotic and necrotic cells by dual stain acridine orange/ethidium bromide

The dual AO and EtBr stains were mixed with treated cells MCF-7 and PC-3. In the cell membrane, viable cells were intact with AO dye and eliminated the EtBr. However, the treated MCF-7 and PC-3 cells have absorbed EtBr stain because of disrupted membranes. EtBr stain reached toward nuclei and gave a red/orange color indication as shown in Figure 6a and b. However, in control, MCF-7 and PC-3 cells show large green nuclei under fluorescent microscopy ×400.

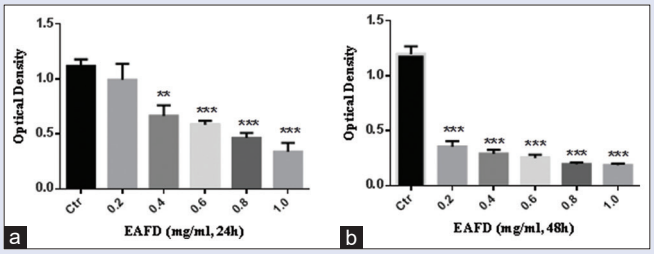

Figure 1: Established dose-dependent cell anti-proliferation at 24 h (a) and 48 h (b) was demonstrated. The log inhibition versus the variable response slope (four parameters) using software Prism graph pad 6.0 was statistically analyzing ethyl acetate fraction of dill antiproliferative activities in MCF-7 cells. Mean ± triplicate standard error of the mean values have been shown. The *P* value is ** and *** respectively $P < 0.01$ and $P < 0.001$

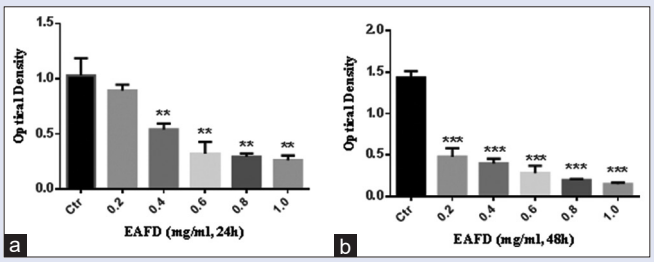

Figure 2: Demonstrated dose-based cell anti-proliferation at 24 h (a) and 48 h (b) controls. A statistical study was done by using Prism graph pad 6.0 software to evaluate ethyl acetate fraction of dill antiproliferative activity in PC-3 cells by the log inhibition versus variable response slope (four parameters). Mean ± triplicate standard error of the mean values have been shown. The *P* value is ** and *** respectively $P < 0.01$ and $P < 0.001$

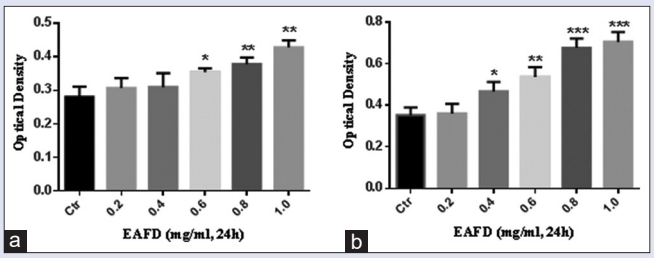

Figure 3: Ethyl acetate fraction of dill induced reactive oxygen species aggregation (DCFH-DA stain) for MCF-7 cells and PC-3 cells and intracellular reactive oxygen species level production. Cells were handled for 24 h (a) PC-3 (b) MCF-7 cells at different concentration of ethyl acetate fraction of dill. Statistically, data were evaluated by using Prism graph pad 6.0 program utilizing log inhibition and variable response slope (4 parameters), the relevant values were found to be a medium ± standard error of the mean The *P* value as seen in ** and ***$P < 0.05$ respectively $P < 0.01$ and $P < 0.001$

Ethyl acetate fraction of dill induced apoptosis by fluorescent nuclear 4,6-diamidino-2-phenylindole stain

The MCF-7 and PC-3 cells were stained with nuclear DAPI stain, after the treatment with EAFD different concentrations. The

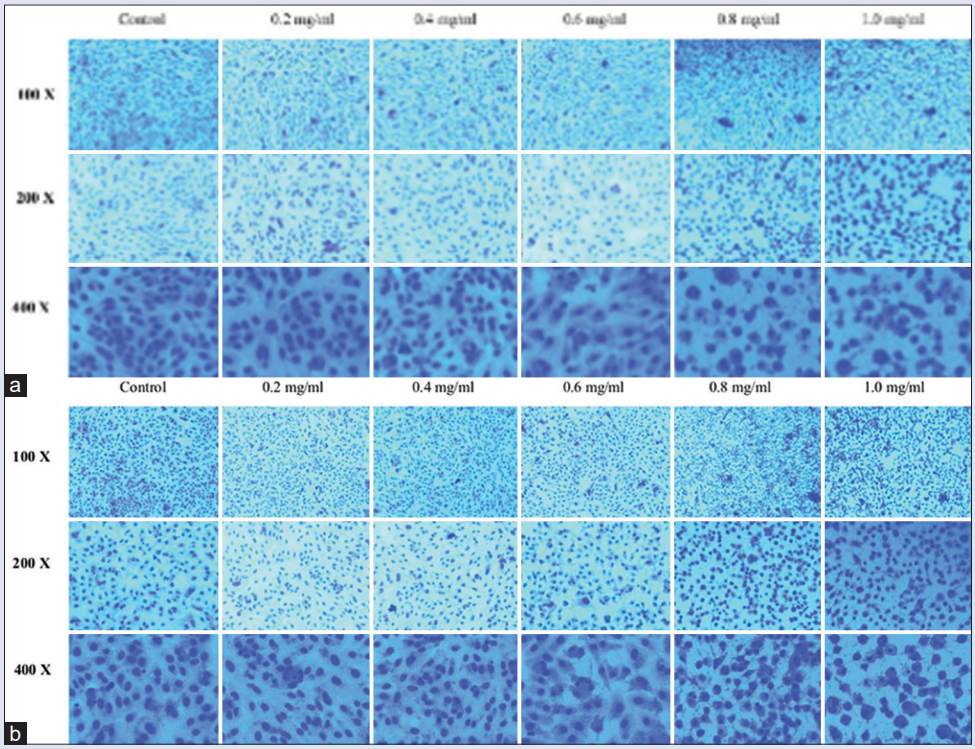

Figure 4: (a) Ethyl acetate fraction of dill treated cells with morphological changes. MCF-7 cells with different ethyl acetate fraction of dill concentrations after 24 h of treatment. (b) PC-3 cells demonstrated morphological changes, including cell shrinkage and blebbing, DNA fragmentation and cell detachment, after 24 h of treatment at various ethyl acetate fraction of dill concentrations. The portraits are taken after staining with Giemsa in ×100, ×200 and ×400 on phase-contrast microscopy

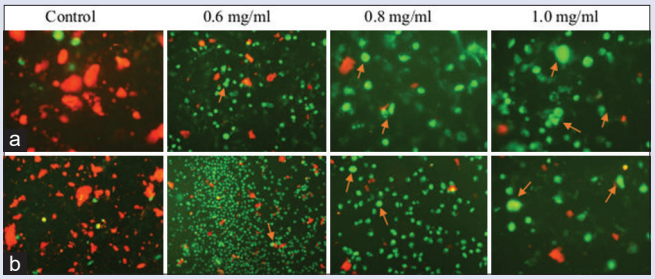

Figure 5: (a) For 24 h and ethyl acetate fraction of dill treatment, the MCF-7 cells were stained with JC-1 dye, characterized by a stained cell magnification of ×400 under a fluorescent microscope. (b) The ethyl acetate fraction of dill treatment was performed on the PC3 cells for 24 h and then stained with the JC 1 dye, followed by a ×400 magnification on the stained cells under a fluorescent microscope

characteristic features of apoptotic cells in the EAFD treatment were nuclear fragmentation, margination of a nucleus, and chromatin condensation at concentrations of 0.6 mg/ml, 0.8 mg/ml and 1.0 mg/ml (red marked arrows) and in control, no apoptotic cells were observed as depicted in Figure 7a and b. The nuclear DAPI staining was observed under fluorescence microscopy ×400.

Molecular docking analysis

Validation of the molecular docking procedure implemented in this study was performed as described earlier. The cognate ligands DRO and N3C, which were bound in the X-ray crystal structures of the respective proteins of Bcl-2 and Bcl-xL, were extracted and re-docked. The poses of bound and re-docked ligands to proteins were compared and RMSDs (root mean square deviations) were calculated [Supplementary Figure 1]. We found that the RMSD values of the re-docking of DRO to Bcl-2 and N3C to Bcl-xL were 0.3842 and 0.7688 Å, respectively. Since the RMSD values were less than the acceptable limit of 2.0 Å, we were confident of adopting the docking protocol for predicting the binding of anethole and carvone to Bcl-2 and Bcl-xL, respectively.

The molecular docking between anethole and carvone with Bcl-2 was performed using Autodock 4.2 and compared with the binding of its cognate ligand, i.e., DRO [Table 1, Figure 8 and Supplementary Figure 2]. We found that both anethole and carvone occupied a similar position at the Bcl-2 binding site, as occupied by the cognate ligand DRO [Figure 8a, b and Supplementary Figure 2a, b]. An analysis of the interaction between anethole and Bcl-2 revealed that the anethole-Bcl-2 complex was stabilized five hydrophobic interactions with Tyr67, Phe71, Met74, Leu96, and Ala108 [Table 1]. Further, the anethole-Bcl-2 complex was stabilized by several other residues (Asp70, Val92, Glu95, and Phe112) forming van der Waals' interaction [Figure 8c]. Similarly, the carvone-Bcl-2 complex was stabilized by twelve hydrophobic interactions with Phe63, Tyr67, Phe71, Met74, Val92, Leu96, Ala108, and Phe112 [Table 1]. Moreover, some other residues such as Asp70 and Phe109 formed van der Waals' interactions to stabilize the carvone-Bcl-2 complex [Figure 8d]. Comparatively, an analysis of the interaction between DRO. Moreover, Bcl-2 revealed that the DRO-Bcl-2 complex was stabilized by one hydrogen bond and one electrostatic interaction with Asp70 [Supplementary Figure 2c]. Furthermore, DRO. Formed eleven hydrophobic interactions with Val92, Phe63, Tyr67, Phe71, Met74, Leu96, Arg105, and Ala108 [Table 1]. Further, the DRO-Bcl-2 complex was stabilized by several residues (Arg88, Glu95, Gly104, and Phe112) forming van der Waals' interaction [Supplementary Figure 2c]. The binding energies and the corresponding binding affinity of DRO,

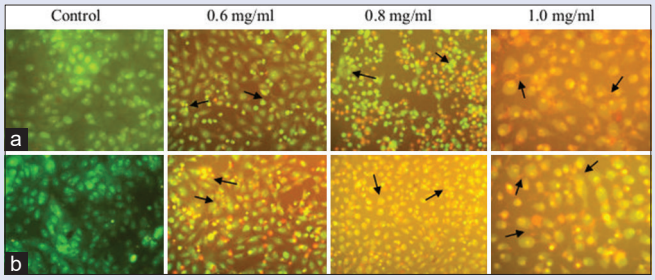

Figure 6: (a) Ethyl acetate fraction of dill -treated MCF-7 cells in the dual dye, acridine orange and bromide ethidium (EtBr) were stained for 24 h. (b) Ethyl acetate fraction of dill -treated PC-3 cells were stained with dual colour dye, acridine orange and ethidium bromide for the 24-h duration of incubation were subsequently observed under a fluorescent microscope ×400 magnification

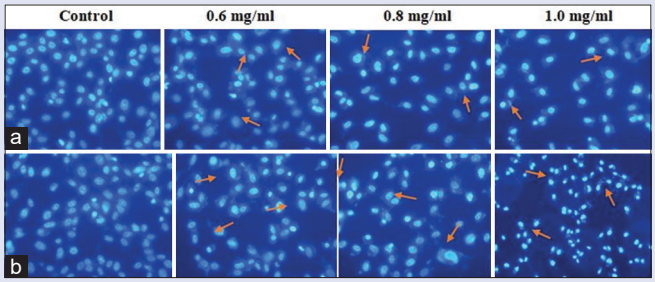

Figure 7: (a) Ethyl acetate fraction of dill was employed in MCF-7 cells for 24 h and then stained with nuclear 4,6-diamidino-2-phenylindole stain and the fluorescent microscope labeled ×400 found 4,6-diamidino-2-phenylindole cell. (b) PC-3 cells were handled for 24 h with ethyl acetate fraction of dill and subsequently stained with 4,6-diamidino-2-phenylindole nuclei, later found ×400 magnifying under a fluorescent microscope

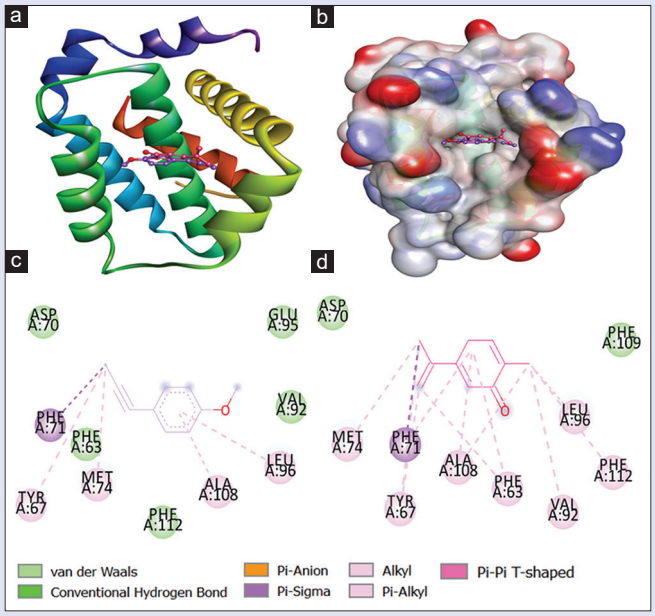

Figure 8: Molecular docking analysis of the interaction between anethole and carvone with Bcl-2 protein. (a) 2D representation of the binding of anethole (purple) and carvone (pink) to Bcl-2. (b) 3D representation of the binding of anethole (purple) and carvone (pink) to the binding cavity of Bcl-2. (c) Involvement of various amino acid residues and different interaction forces between anethole and Bcl-2 and (d) Involvement of various amino acid residues and different interactions between carvone and Bcl-2

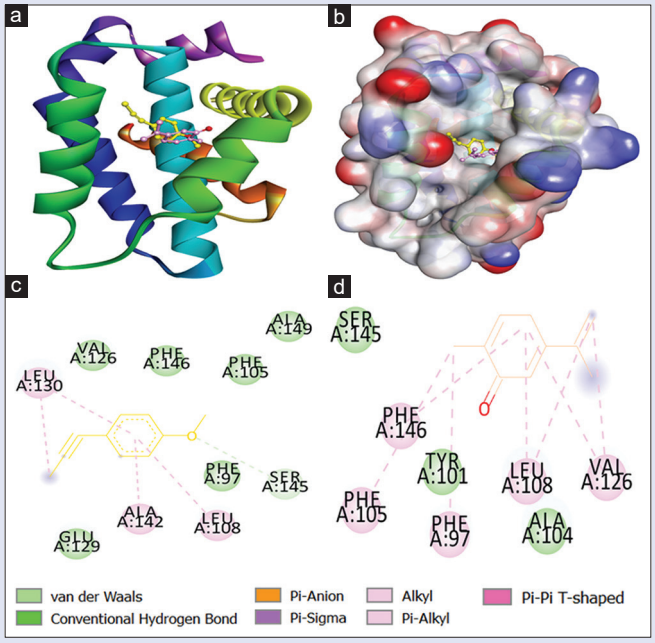

Figure 9: Molecular docking analysis of the interaction between anethole and carvone with Bcl-xL protein. (a) 2D representation of the binding of anethole (yellow) and carvone (light pink) to Bcl-xL. (b) 3D representation of the binding of anethole (yellow) and carvone (light pink) to the binding cavity of Bcl-xL. (c) Involvement of various amino acid residues and different interaction forces between anethole and Bcl-xL. (d) Involvement of various amino acid residues and different interactions between carvone and Bcl-xL

anethole, and carvone toward Bcl-2 were estimated to be−10.2 kcal mol^{-1} and 3.03×10^{7} M^{-1}, −5.1 kcal mol^{-1} and 5.05×10^{3} M^{-1} and −5.5 kcal mol^{-1} and 1.08×10^{4} M^{-1}, respectively [Table 1]. It is interesting to note that the amino acid residues Tyr67, Phe71, Met74, Leu96, and Ala108 of Bcl-2 were common in their interaction with anethole and DRO, while the residues Phe63, Tyr67, Phe71, Met74, Val92, Leu96, and Ala108 were commonly involved in the interaction with carvone and DRO.

Similarly, the molecular docking between anethole and carvone with Bcl-xL was performed using Autodock 4.2 and compared with the binding of its cognate ligand, i.e., N3C [Table 1, Figure 9 and Supplementary Figure 3]. We found that both anethole and carvone occupied a similar position at the Bcl-xL binding site, as occupied by the cognate ligand N3C [Figure 9a, b and Supplementary Figure 3a, b]. An analysis of the interaction between anethole and Bcl-xL revealed that the anethole-Bcl-xL complex was stabilized one carbon-hydrogen bond with Ser145 and four hydrophobic interactions with Leu108, Leu130, and Ala142 [Table 1]. Further, the anethole-Bcl-xL complex was stabilized by several other residues (Phe97, Phe105, Val126, Glu129, Phe146, and Ala149) forming van der Waals' interaction [Figure 9c]. Similarly, the carvone-Bcl-xL complex was stabilized by seven hydrophobic interactions with Phe97, Phe105, Val126, and Phe146 [Table 1]. Moreover, some other residues such as Tyr101, Ala104, and Ser145 formed van der Waals' interactions to stabilize the carvone-Bcl-xL complex [Figure 9d]. Comparatively, an analysis of the interaction between N3C and Bcl-xL revealed that the N3C-Bcl-xL complex was stabilized by three hydrogen bonds with Asn136, Gly138, and Asn197.

Table 1: Molecular docking between anethole and carvone with Bcl-2 and Bcl-xL

Donor atoms	Acceptor atom	Distance (Å)	Type of interaction	Binding free energy, ΔG (kcal/mol)	Binding affinity, K_d/(M)
Bcl-2 and DRO*					
Lig: N	ASP70:OD2	2.9553	Conventional hydrogen bond	−10.2	3.03×10^{7}
ASP70:OD2	Lig	4.8135	Electrostatic (Pi-Anion)		
MET74:CE	Lig	3.5674	Hydrophobic (Pi-Sigma)		
LEU96:CD1	Lig	3.8681	Hydrophobic (Pi-Sigma)		
Lig: C	TYR67	3.5199	Hydrophobic (Pi-Sigma)		
PHE63	Lig	5.2880	Hydrophobic (Pi-Pi T-shaped)		
PHE71	Lig	4.9682	Hydrophobic (Pi-Pi T-shaped)		
Lig: C	LEU96	4.9539	Hydrophobic (Alkyl)		
Lig	ARG105	5.2941	Hydrophobic (Pi-Alkyl)		
Lig	ALA108	4.4414	Hydrophobic (Pi-Alkyl)		
Lig	LEU96	5.1674	Hydrophobic (Pi-Alkyl)		
Lig	ALA108	4.4935	Hydrophobic (Pi-Alkyl)		
Lig	VAL92	5.0873	Hydrophobic (Pi-Alkyl)		
Bcl-2 and Anethole					
Lig: C	PHE71	3.6212	Hydrophobic (Pi-Sigma)	−5.1	5.05×10^{3}
Lig: C	MET74	5.2059	Hydrophobic (Alkyl)		
TYR67	Lig: C	5.2673	Hydrophobic (Pi-Alkyl)		
Lig	LEU96	5.0944	Hydrophobic (Pi-Alkyl)		
Lig	ALA108	4.6867	Hydrophobic (Pi-Alkyl)		
Bcl-2 and Carvone					
Lig: C	PHE71	3.6680	Hydrophobic (Pi-Sigma)	−5.5	1.08×10^{4}
ALA108	Lig	4.4649	Hydrophobic (Alkyl)		
ALA108	Lig: C	4.3899	Hydrophobic (Alkyl)		
Lig: C	VAL92	4.9689	Hydrophobic (Alkyl)		
Lig: C	LEU96	3.7219	Hydrophobic (Alkyl)		
Lig: C	MET74	5.3514	Hydrophobic (Alkyl)		
PHE63	Lig	5.1544	Hydrophobic (Pi-Alkyl)		
PHE63	Lig: C	4.9114	Hydrophobic (Pi-Alkyl)		
TYR67	Lig: C	5.0980	Hydrophobic (Pi-Alkyl)		
TYR67	Lig: C	3.6976	Hydrophobic (Pi-Alkyl)		
PHE71	Lig	4.8662	Hydrophobic (Pi-Alkyl)		
PHE112	Lig: C	4.7778	Hydrophobic (Pi-Alkyl)		
Bcl-xL and N3C#					
ASN136:HD22	Lig: O	2.6059	Conventional Hydrogen Bond	−11.2	1.64×10^{8}
GLY138:HN	Lig: O	2.8400	Conventional Hydrogen Bond		
Lig: C	ASN197:O	3.6727	Carbon Hydrogen Bond		
LEU130:CD1	Lig	3.7629	Hydrophobic (Pi-Sigma)		
Lig	TYR195	4.1832	Hydrophobic (Pi-Pi Stacked)		
Lig	PHE97	5.3298	Hydrophobic (Pi-Pi T-shaped)		
Lig: Cl	LEU108	5.1271	Hydrophobic (Alkyl)		
Lig	ALA93	5.3334	Hydrophobic (Pi-Alkyl)		
Lig	VAL141	4.6272	Hydrophobic (Pi-Alkyl)		
Lig	ARG139	4.9049	Hydrophobic (Pi-Alkyl)		
Lig	LEU108	4.9956	Hydrophobic (Pi-Alkyl)		
Lig	ALA142	4.9785	Hydrophobic (Pi-Alkyl)		
PHE97	Lig: Cl	5.4378	Hydrophobic (Pi-Alkyl)		
PHE105	Lig: Cl	4.3682	Hydrophobic (Pi-Alkyl)		
Bcl-xL and Anethole					
SER145:CB	Lig: O	3.78821	Carbon Hydrogen Bond	−6.0	2.52×10^{4}
Lig: C	LEU130	4.43955	Hydrophobic (Alkyl)		
Lig	LEU108	5.15788	Hydrophobic (Pi-Alkyl)		
Lig	LEU130	5.24962	Hydrophobic (Pi-Alkyl)		
Lig	ALA142	4.84907	Hydrophobic (Pi-Alkyl)		
Bcl-xL and Carvone					
VAL126	Lig	5.41712	Hydrophobic (Alkyl)	−6.2	3.53×10^{4}
Lig	LEU108	3.79128	Hydrophobic (Alkyl)		
Lig: C	LEU108	4.46979	Hydrophobic (Alkyl)		
Lig: C	VAL126	4.25917	Hydrophobic (Alkyl)		
PHE97	Lig: C	5.08426	Hydrophobic (Pi-Alkyl)		
PHE105	Lig: C	4.48069	Hydrophobic (Pi-Alkyl)		
PHE146	Lig	5.33908	Hydrophobic (Pi-Alkyl)		

*Chemically DRO is 1-(2-[(3S)-3-(aminomethyl)-3,4-dihydroisoquinolin-2 (1H)-yl] carbonylphenyl) -4-chloro-5-methyl-N, N-diphenyl-1H-pyrazole-3-carboxamide; #Chemically N3C is 4-4-[(4'-chlorobiphenyl-2-yl) methyl] piperazin-1-yl-N-[4-((1R)-3-(dimethylamino)-1-[(phenylthio) methyl] propyl} amino)-3-nitrophenyl] sulfonylbenzamide

Furthermore, N3C formed eleven hydrophobic interactions with Ala93, Phe97, Phe105, Leu108, Leu130, Arg139, Val141, Ala142, and Tyr195 [Supplementary Figure 3c and Table 1]. Further, the N3C-Bcl-xL complex was stabilized by several other residues (Glu96, Arg100, Tyr101, Val126, Glu129, Trp137, Ser145, Phe146, and Ala149) forming van der Waals' interaction [Supplementary Figure 3c]. The binding energies and the corresponding binding affinity of N3C, anethole, and carvone toward Bcl-xL were estimated to be−11.2 kcal mol^{-1} and 1.64×10^8 M^{-1}, −6.0 kcal mol^{-1} and 2.52×10^4 M^{-1} and−6.2 kcal mol^{-1} and 3.53×10^4 M^{-1} respectively [Table 1]. Interestingly, the amino acid residues Leu108 and Leu130 of Bcl-xL were commonly involved in interacting with carvone and N3C, while the residues Phe97, Phe105, and Leu108 were widely applied in making contact with carvone and N3C.

DISCUSSION

The medicinal herbs have been serving as an excellent source for the discovery of novel, potential and reliable anticancer agents; indeed, over 60% of anticancer drugs available in the market today are either derived directly from natural compounds or are a modified natural product compound.[24] Moreover, the growing use of secondary metabolites derived from medicinal herbs and other natural products in the treatment of cancer has gained tremendous momentum in the recent few years.[25] Furthermore, the production of enzymes from medicinal plants and its constituents stimulate the antitumor activity by suppressing cancer's stimulating enzymes, thereby leading to antioxidant effects in different cancer cell lines potentially.

A. graveolens is being used in the treatment of various disorders and ailments; it has shown mucosal protective, anti-secretory effects, and free radical scavenging properties.[26] In this study, the antiproliferative activity of EAFD on MCF-7 and PC-3 cell lines was investigated by time- and dose-dependent manner. The 24 h treatment of EAFD has shown a significant decline in the percentage of viable cell numbers in both the cell lines used. Furthermore, 48 h of EAFD treatments with MCF-7 and PC-3 cells have shown a significant decrease in the percentages of viable cell numbers with an increase in time. Interestingly, it was evident in both the cell lines that 48 h of EAFD treatments portrays that the increase in exposure time is leading to an increase in the anti-proliferation effects simultaneously. It has been previously reported that *A. graveolens* displayed antiproliferative activity in the HepG2 cell line effectively.

Dietary herbs are inevitable sources of a wide variety of bioactive antioxidant compounds, which can neutralize the free radicals and oxidative stress properties in cancer cells. The plasma membrane gets disrupts by an increased level of ROS and targets the cytoskeleton and then damages the DNA of the cell altogether called oxidative stress.[27] Thus, to develop the therapeutic agents from dietary herbs, the study of individual bioactive components is of considerable significance. Numerous previous reports have shown that natural products have targeted the cancer cell with increased ROS, which attenuates cancer cell growth. The regulation levels of ROS play a significant role in inducing apoptotic cell death. The treatments of EAFD with MCF-7 cells have shown significant antiproliferative effects with an increase in concentrations both in the dose and time-dependent manner. Nevertheless, the PC-3 cell line shows significant quiet results after EAFD treatment at similar concentrations in time- and dose-dependent style when compared to MCF-7 cells. Moreover, the treatment of EAFD in these cell lines has increased the generation of ROS-mediated cell damage and subsequently exhibited antiproliferative activity *in vitro*.

The EAFD delineated various cellular and morphological changes such as blebbing, cell shrinkage, compact cell organelles, dense cytoplasm, loss of cell integrity, condensed nuclei, and cell adherence in MCF-7 cells and PC-3 cells. It was evident that EAFD induces early and late apoptosis. Mitochondria, possibly a crucial apoptosis control, has shown involvement in dissipation and integration of MMP various pro-apoptotic mechanisms through the release of cytochrome 'C' into the cytosol, which activates the caspases and later leads to cell death.[28] The JC-1 dye is accumulating inside mitochondria after losing its integrity in the mitochondrial region that gives a clear picture between viable cells and apoptotic cells. The treatment of EAFD in MCF-7 and PC-3 cells afterward stained with JC-1 dye, it indicates that degradation of the mitochondrial membrane. Another previous study shows that the apoptotic inducing effect of estragole isolated from Fennel seeds has a resemblance to our results.

In addition, dual stain Acridine orange (AO) and EtBr fluorescence dyes were used. When the cytoplasmic membrane loses integrity, EtBr stains the nuclei alone releasing red color signal, but in AO stain, only viable cells give a green fluorescence signal.

The mixed stain AO/EtBr were categorized into four different types, the cells after staining as follows: normal green nucleus appears in living cells, a bright green nucleus with fragmented or condensed chromatin appears in early apoptotic cells whereas, uniformly orange stained cells nuclei appear in necrotic cells.[29] Dual mixed stain AO/EtBr was used to stain with untreated cells which had produced a normal green color fluorescence signal. Whereas, the treated MCF-7 and PC-3 cells with EAFD of concentrations of 0.8 mg/ml and 1.0 mg/ml produced orange/red color fluorescence signal, which indicates that early and late apoptosis of cells. The characteristic feature of nuclei about apoptotic cells is that they have shown a red intense fluorescence signal, which depicts either necrosis or late apoptosis.

The nuclear DAPI stain was used to detect nuclear morphological changes in apoptotic cells associated with nuclear fragmentation, chromatin condensation, and cytoplasmic condensation followed by complete degradation in the nucleus.[30] The MCF-7 and PC-3 cells were treated with EAFD followed by DAPI staining, which helps in the detection of apoptotic bodies with chromatin condensation, nuclear fragmentation and also degradation of nuclei. The mode of apoptotic cell death gives a blue color signal in the fluorescence microscope.

The defect in apoptotic machinery which provides survival advantages is a common observation in various kinds of cancers. Thus, identifying novel molecules that activate apoptosis is a viable approach to target cancer cells. The anti-apoptotic proteins Bcl-2 and Bcl-xL of the BCL-2 protein family are attractive drug targets as these proteins are generally overexpressed in many tumors. In this study, we performed molecular docking between the two most abundant components of EAFD, i.e., anethole and carvone with anti-apoptotic proteins Bcl-2 and Bcl-xL. Analyses of docking results suggest that anethole and carvone bind to the hydrophobic patches of Bcl-2 and Bcl-xL through hydrophobic interactions. Anethole and carvone interact with the key residues of Bcl-2 protein (Phe63, Tyr67, Phe71, Met74, Val92, Leu96, and Ala108) and Bcl-xL protein (Phe97, Phe105, Leu108, and Leu130). Our results are in agreement with the findings of Sathishkumar *et al.* (2012) that the potential inhibitors of Bcl-2 and Bcl-xL bind at the surface exposed hydrophobic patches.[31]

CONCLUSION

We found that the level of intracellular oxidative stress (ROS) is increased and EAFD confirms the following degradation of the mitochondrial membrane, chromatin condensation, nuclear fragmentation and even nuclei degradation based on our fluorescent staining dye. This result suggests that EAFD may be antiproliferative activity and leading to pro-apoptotic cell death. The molecular docking analysis also supports this *in-vitro* result.

Financial support and sponsorship

MFA and MTR acknowledge the generous support from the Research Supporting Project (No. RSP-2021-122) by King Saud University, Riyadh, Kingdom of Saudi Arabia.

Conflicts of interest

There are no conflicts of interest.

REFERENCES

1. Luebeck EG, Curtius K, Jeon J, Hazelton WD. Impact of tumor progression on cancer incidence curves. Cancer Res 2013;73:1086-96.
2. Niculescu VF. Carcinogenesis: Recent insights in protist stem cell biology lead to a better understanding of atavistic mechanisms implied in cancer development. MOJ Tumor Res 2018;1:18-29.
3. Global Burden of Disease Cancer Collaboration; Fitzmaurice C, Allen C, Barber RM, Barregard L, Bhutta ZA, *et al.* Global, regional, and national cancer incidence, mortality, years of life lost, years lived with disability, and disability-adjusted life-years for 32 cancer groups, 1990 to 2015: A systematic analysis for the global burden of disease study. JAMA Oncol 2017;3:524-48.
4. The International Agency for Research on Cancer (IARC) Report W. Latest Global Cancer Data: Cancer Burden Rises to 18.1 Million New Cases and 9.6 Million Cancer Deaths in 2018. Int Agency Res Cancer 2018. Available form: https://www.iarc.who.int/wp-content/uploads/2018/09/pr263_E.pdf. [Last accessed on 2019 Feb 20].
5. Roy PS, Saikia BJ. Cancer and cure: A critical analysis. Indian J Cancer 2016;53:441-2.
6. Petrovska B. Historical review of medicinal plants' usage. Pharmacogn Rev 2012;6:1.
7. Mohammed FA, Razvi SS, Abdul WM, Mohammed K, Hakeem KR, Banaganapalli B, *et al.* Protective Role of Medicinal Herb *Anethum graveolens* (Dill) Against Various Human Diseases and Metabolic InPlant and Human Health, 2019:181-94.
8. Kojuri J, Vosoughi AR, Akrami M. Effects of *Anethum graveolens* and garlic on lipid profile in hyperlipidemic patients. Lipids Health Dis 2007;6:5.
9. Goodarzi MT, Khodadadi I, Tavilani H, Abbasi Oshaghi E. The role of *Anethum graveolens* L. (Dill) in the management of diabetes. J Trop Med 2016;2016:1-11.
10. Naseri M, Mojab F, Khodadoost M, Kamalinejad M, Davati A, Choopani R, *et al.* The study of anti-inflammatory activity of oil-based dill (*Anethum graveolens* L.) extract used topically in formalin-induced inflammation male rat paw. Iran J Pharm Res 2012;11:1169-74.
11. Ramadan M, Abd-Algader N, El-kamali H, Farrag AH, Ghanem K. Volatile compounds and antioxidant activity of the aromatic herb *Anethum graveolens*. J Arab Soc Med Res 2013;8:79.
12. Larijani B, Esfahani MM, Moghimi M, Shams Ardakani MR, Keshavarz M, Kordafshari G, *et al.* Prevention and treatment of flatulence from a traditional persian medicine perspective. Iran Red Crescent Med J 2016;18:e23664.
13. Adams JM, Cory S. The Bcl-2 arbiters of apoptosis and their growing role as cancer targets. Cell Death Differ 2018;25:27-36.
14. Hanahan D, Weinberg RA. Hallmarks of cancer: The next generation. Cell 2011;144:646-74.
15. Zhai D, Ke N, Zhang H, Ladror U, Joseph M, Eichinger A, *et al.* Characterization of the anti-apoptotic mechanism of Bcl-B. Biochem J 2003;376:229-36.
16. Petros AM, Olejniczak ET, Fesik SW. Structural biology of the Bcl-2 family of proteins. Biochim Biophys Acta Mol Cell Res 2004;1644:83-94.
17. Mohammed FA, Elkady AI, Syed FQ, Mirza MB, Hakeem KR, Alkarim S. *Anethum graveolens* (dill) – A medicinal herb induces apoptosis and cell cycle arrest in HepG2 cell line. J Ethnopharmacol 2018;219:15-22.
18. Arıcan GO. Effects of Geven root extract on proliferation of HeLa cells and bcl-2 gene expressions. African J Biotechnol 2012;11:4296-304.
19. Porter J, Payne A, de Candole B, Ford D, Hutchinson B, Trevitt G, *et al.* Tetrahydroisoquinoline amide substituted phenyl pyrazoles as selective Bcl-2 inhibitors. Bioorg Med Chem Lett 2009;19:230-3.
20. Lee EF, Czabotar PE, Smith BJ, Deshayes K, Zobel K, Colman PM, *et al.* Crystal structure of ABT-737 complexed with Bcl-xL: Implications for selectivity of antagonists of the Bcl-2 family. Cell Death Differ 2007;14:1711-3.
21. Rehman MT, Shamsi H, Khan AU. Insight into the binding mechanism of imipenem to human serum albumin by spectroscopic and computational approaches. Mol Pharm 2014;11:1785-97.
22. Rabbani N, Tabrez S, Islam BU, Rehman MT, Alsenaidy AM, AlAjmi MF, *et al.* Characterization of colchicine binding with normal and glycated albumin: *In vitro* and molecular docking analysis. J Biomol Struct Dyn 2018;36:3453-62.
23. Rehman MT, Ahmed S, Khan AU. Interaction of meropenem with 'N' and 'B' isoforms of human serum albumin: A spectroscopic and molecular docking study. J Biomol Struct Dyn 2016;34:1849-64.
24. Cragg GM, Newman DJ. Plants as a source of anti-cancer agents. J Ethnopharmacol 2005;100:72-9.
25. Newman DJ, Cragg GM. Natural products as sources of new drugs over the 30 years from 1981 to 2014. J Nat Prod 2016;79:629-61.
26. Saleh-E-In MM, Sultana N, Hossain MN, Hasan S, Islam MR. Pharmacological effects of the phytochemicals of *Anethum sowa* L. root extracts. BMC Complement Altern Med 2016;16:464.
27. Redza-Dutordoir M, Averill-Bates DA. Activation of apoptosis signalling pathways by reactive oxygen species. Biochim Biophys Acta 2016;1863:2977-92.
28. Syed FQ, Elkady AI, Mohammed FA, Mirza MB, Hakeem KR, Alkarim S. Chloroform fraction of *Foeniculum vulgare* induced ROS mediated, mitochondria-caspase-dependent apoptotic pathway in MCF-7, human breast cancer cell line. J Ethnopharmacol 2018;218:16-26.
29. Ribble D, Goldstein NB, Norris DA, Shellman YG. A simple technique for quantifying apoptosis in 96-well plates. BMC Biotechnol 2005;5:12.
30. Mandelkow R, Gümbel D, Ahrend H, Kaul A, Zimmermann U, Burchardt M, *et al.* Detection and quantification of nuclear morphology changes in apoptotic cells by fluorescence microscopy and subsequent analysis of visualized fluorescent signals. Anticancer Res 2017;37:2239-44.
31. Sathishkumar N, Sathiyamoorthy S, Ramya M, Yang DU, Lee HN, Yang DC. Molecular docking studies of anti-apoptotic Bcl-2, Bcl-xL, and MCL-1 proteins with ginsenosides from Panax ginseng. J Enzyme Inhib Med Chem 2012;27:685-92.